electronics

MDPI

Article

Predicting the Frequency Characteristics of Hybrid Meander Systems Using a Feed-Forward Backpropagation Network

Darius Plonis [1], Andrius Katkevičius [1], Audrius Krukonis [1], Vaiva Šlegerytė [1], Rytis Maskeliūnas [2] and Robertas Damaševičius [3,*]

1 Department of Electronic Systems, Vilnius Gediminas Technical University, 03227 Vilnius, Lithuania; darius.plonis@vgtu.lt (D.P.); andrius.katkevicius@vgtu.lt (A.K.); audrius.krukonis@vgtu.lt (A.K.); vaiva.slegeryte@vgtu.lt (V.Š.)

2 Centre of Real Time Computer Systems, Kaunas University of Technology, 51423 Kaunas, Lithuania; rytis.maskeliunas@ktu.lt

3 Department of Software Engineering, Kaunas University of Technology, 51368 Kaunas, Lithuania

* Correspondence: robertas.damasevicius@ktu.lt; Tel.: +370-37-300353

Received: 12 December 2018; Accepted: 7 January 2019; Published: 11 January 2019

Abstract: The process of designing microwave devices is difficult and time-consuming because the analytical and numerical methods used in the design process are complex. Therefore, it is necessary to search for new methods that will allow for an acceleration of synthesis and analytic procedures. This is especially important in cases where the procedures of synthesis and analysis have to be repeated many times, until the correct device configuration is found. Artificial neural networks are one of the possible alternatives for the acceleration of the design process. In this paper we present a procedure for analyzing a hybrid meander system (HMS) using the feed-forward backpropagation network (FFBN). We compared the prediction results of the transmission factor $S_{21}(f)$ and the reflection factor $S_{11}(f)$, obtained using the FFBN, with results obtained using traditional analytical and numerical methods, as well as with experimental results. The comparisons show that prediction results significantly depend on the FFBN structure. In terms of the lowest difference between the characteristics calculated using the method of moments (MoM) and characteristics predicted using the FFBN, the best prediction was achieved using the FFBN with three hidden layers, which included 18 neurons in the first hidden layer, 14 neurons in the second hidden layer, and 2 neurons in the third hidden layer. Differences between the predicted and calculated results did not exceed 7% for the $S_{11}(f)$ parameter and 5% for the $S_{21}(f)$ parameter. The prediction of parameters using the FFBN allowed the analysis procedure to be sped up from hours to minutes. The experimental results correlated with the predicted characteristics.

Keywords: hybrid meander system; microwave device; receiver antenna; feed-forward backpropagation network; artificial neural network

1. Introduction

The manufacture of microwave devices usually consists of several stages: (1) synthesis of physical and geometrical parameters using analytical and numerical iterative methods [1–4], (2) analysis of synthesized models using analytical and numerical iterative methods [5–9], and (3) experimental verification [10–14]. This procedure is usually time consuming, especially when the approximate parameters are not known and many synthesis iterations are required [15,16]. The most time-consuming stage is the repetition of experimental verification, as this requires the manufacturing of another experimental prototype of the device. A less time-consuming alternative is to repeat the analysis of the synthesized model. However, this still requires substantial time and can take

many hours [17,18]. Calculation time using the analytical methods is quite short, but the preparation procedure and the development of a specific mathematical model for every particular design of a microwave device is a long process and requires a great deal of domain knowledge [6].

Recently, artificial neural networks (ANNs) were successfully used for modeling microwave devices [19–22]. ANNs have been used in both synthesis and analysis [23–25]. The advantage of using ANNs is the elimination of complex analytical and numerical iterative calculations, which allow for a quicker manufacturing of microwave devices. The disadvantage of ANNs, on the other hand, may be their long training time, which depends on training data, training algorithms, and the initial selection of connection weights [26].

The parametric optimization of a microwave device can also be performed using evolutionary optimization methods such as genetic algorithms (GAs) [27–29], but such methods are slow and may have convergence problems.

The analysis and synthesis procedures of a particular design of meander microwave systems may take from several minutes up to several days [30]. In most cases, it is not possible to extract the appropriate parameters of the meander system the first time. In this way, the entire design cycle of the meander system can take even longer, as it is necessary to find the optimal design parameters of the meander system in the synthesis stage of investigation through multiple repetitions. Long computation time then becomes a problem [16]. Another problem can arise when the dispersion equation, using analytical methods, has either no solution or several solutions, requiring the selection of the correct one using iterative calculations. These problems could also be solved using neural networks.

Here we propose a new technique based on the use of an ANN to predict characteristics present in meander systems. The main advantage is that the rapid estimation of the design parameters allows the analysis and design of the meander systems to be performed in real-time as opposed to the long computations which are required when using analytical and numerical methods. The particular model of the hybrid meander system used for the investigation [30] included several new modifications, which allowed the use of the analyzed hybrid meander system in small pocket devices. We predicted the electrical parameters of the hybrid meander slow-wave system using the feed-forward backpropagation network (FFBN) and compared the predicted results with the results obtained using analytical and numerical iterative methods, as well as with the results of physical measurements.

2. Materials and Methods

We investigated the hybrid meander slow-wave helical (HMH) system using the analytical multiconductor line and numerical finite-difference time-domain methods. Such meander systems are applied as wide-band slow-wave structures for the retardation of electromagnetic waves in traveling-wave tubes, traveling-wave cathode-ray tubes, delay lines, and other microwave devices.

2.1. Model of the Hybrid Meander Systems

The relatively low characteristic impedance and dispersion of the phase velocity of electromagnetic waves are negative characteristic features of meander systems (Figure 1a). This characteristic impedance was increased by bending the peripheral parts of the meander electrodes and forming the helical turns (Figure 1b,c). Calculations of the hybrid meander system were executed in CST Microwave Studio® (CST MWS) using the finite-difference time-domain method.

The main dimensions of the meander system were as follows: the width of the meander electrode $2a$ = 15 mm, the step of conductors L = 2 mm, the gaps among the conductors l = 0.5 mm, the thickness of conductors t = 0.2 mm, the height of dielectric substrate h = 0.5 mm, and the length of the system L_s = 29.5 mm (Figure 2a,b). The diameter of the turns was d = 2.5 mm. The diameter of the conductors of the turns was the same as the thickness of the meander electrode (0.2 mm).

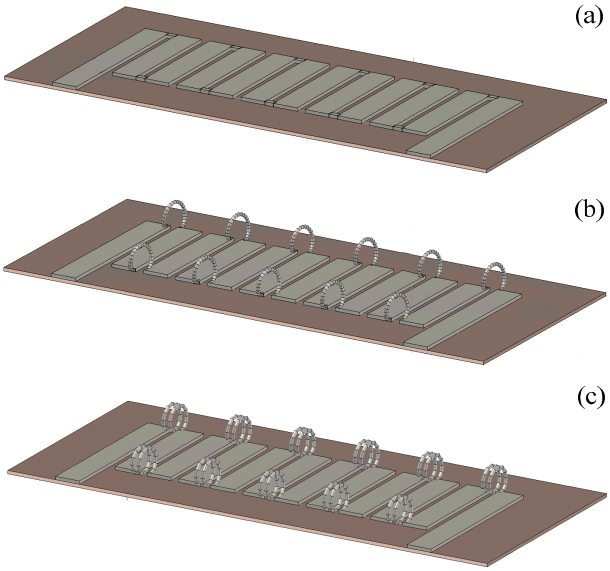

Figure 1. (**a**) Meander system; (**b**) Hybrid meander system with one turn in the peripherals; (**c**) Hybrid meander system with two turns in the peripherals visualized in the CST Microwave Studio® environment.

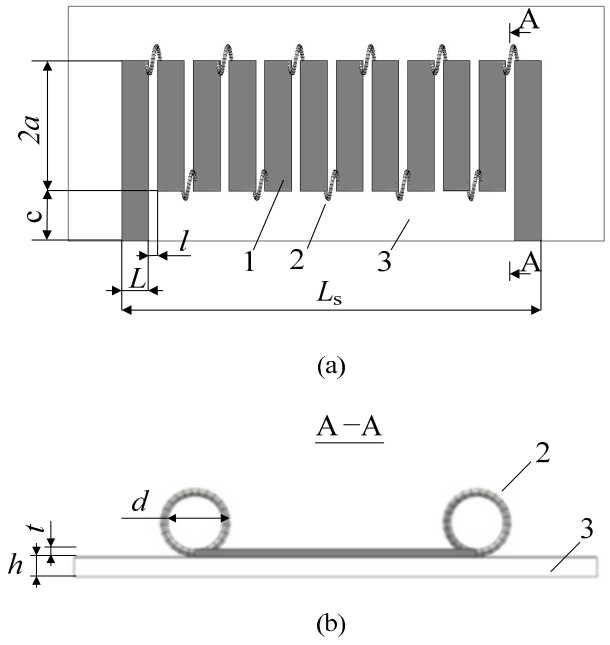

Figure 2. (**a**) Top view of hybrid meander conductor, and (**b**) Cross-view of hybrid meander conductor, where 1 = central meander electrode; 2 = peripheral helical turns of electrode; and 3 = dielectric substrate.

Although the HMH system had better characteristics when compared with an ordinary meander system, it also had some disadvantages. The biggest disadvantage was the use of the peripheral coils of the HMH system, which occupied quite a large amount of space. This was a disadvantage especially when employed in small portable devices. Therefore, we replaced the coils of the peripheral parts with inductive components and evaluated the modification in Sonnet® software (Sonnet Software, Inc., Syracuse, NY, USA) using the method of moments (MoM) (see Figure 3).

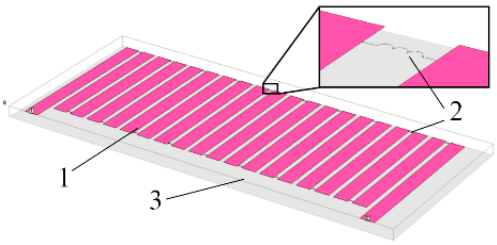

Figure 3. Meander system with inductive components in the peripheral parts, where 1 = central meander electrode; 2 = peripheral helical turns of electrode; and 3 = dielectric substrate.

2.2. Prediction of HMH Characteristics

The electrical properties of the HMH system can be expressed in terms of the S-parameters: S_{21} (transmission factor) and S_{11} (reflection factor). The S-parameters can be predicted when the vector of the electromagnetic wave frequency consists of $f = \{f_{\min};\ \Delta f;\ f_{\max}\}$, where $f_{\min}$ and $f_{\max}$ are the initial boundaries of the vector of the electromagnetic wave frequency and Δf is the step of the electromagnetic wave frequency. The initial boundaries of the vector of the electromagnetic wave frequency are $f_{\min} = 0$ GHz and $f_{\max}$ = 5 GHz, and the step of the frequency is $\Delta f = 0.02$ GHz.

The inductance vector of the helical turns consists of $L_i = \{L_{\min};\ \Delta L;\ L_{\max}\}$, where $L_{\min}$ and $L_{\max}$ are the initial boundaries of the vector of the inductance of the helical turns and ΔL is the step of the inductance of the helical turns. The initial boundaries of the vector of the inductance of the helical turns are $L_{\min}$= 0 nH and $L_{\max}$ = 30 nH, and the step of the vector of the inductance of the helical turns is $\Delta L = 2$ nH.

2.3. Architecture of the FFBN

The structure of the FFBN was selected dependent on training and validation data samples and iterative experiments, and was adapted by changing the number of hidden layers and the number of neurons in each hidden layer (Figure 4). The first hidden layer had a constant number of 18 neurons during all experiments. This was twice as much as the input layer had. The number of neurons in the second and third hidden layers varied from 0 to 15 neurons (the zero value of neurons means that the neural network did not have a corresponding hidden layer). The best structure of the FFBN was selected during experiments. The activation functions of the first, second, and third hidden layers were hyperbolic tangent sigmoid function (tansing(·)). The input layer of the FFBN consisted of nine neurons. The output layer of the FFBN consisted of two neurons for the prediction of the transmission factor ($S_{21}(f)$) and reflection factor ($S_{11}(f)$) characteristics. The activation functions of the output layer neurons were also hyperbolic tangent sigmoid function (tansing(·)). The FFBN was trained with every sample not less than 20 times. The results that best matched with previous results obtained using Sonnet® software were selected for further processing.

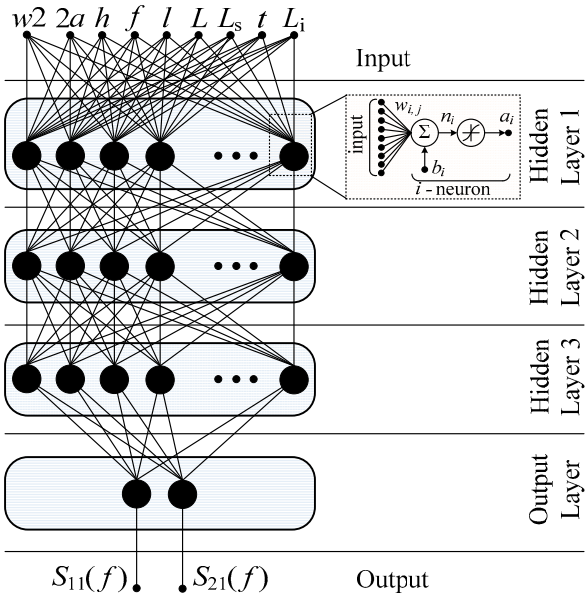

Figure 4. The structure of the feed-forward backpropagation network.

2.4. Training of the FFBN

Samples of frequency characteristics of the HMH system for training the FFBN were collected using Sonnet® software, which performs calculations based on MoM. The HMH model was created in Sonnet® using the following dimensions: the step of conductors (L = 1.5 mm), the gaps between conductors (l = 0.4 mm), the thickness of conductors (t = 0.35 μm), the gap between the meander electrode and the shield ($w2$ = 0.6 mm), the inductance of the helical turns (inductivity of the coils, which varied from 0 to 30 nH with a step of 2 nH), and the frequency of the electromagnetic waves (which varied from 0 to 5 GHz with the step of 0.02 GHz). FR-4 material—a composite material composed of woven fiberglass cloth with an epoxy resin binder—was selected for the dielectric substrate.

The S-parameters of $S_{21}(f)$ (transmission factor) and $S_{11}(f)$ (reflection factor) were calculated with Sonnet® software according to the different values of the inductivity of the peripheral parts of the meander. The calculated data samples were divided into training (70% of samples), validation (15% of samples), and testing (15% of samples) data samples. Every sample consisted of a 1×9 input and a 1×2 target matrix. There were 250 data samples calculated with the Sonnet® software in total. Therefore, the sizes of the input and output matrices were 9×250 and 2×250, respectively. There were 175 data samples used for training, 38 data samples for validation, and 37 data samples for testing. The number of epochs was equal to 1000 by default. The mean squared error (MSE) method was selected for the validation of the network. Other validation methods were not investigated. The performance parameter of MSE was selected by default and was equal to 10^{-4}. The validation was made by the FFBN according to the performance parameter of the MSE—the FFBN changed its weights of connections between neurons until the desired performance parameter was reached.

The training, validation, and testing processes were performed with different configurations of the FFBN. The MSE values (in percentage) of validation with the FFBN consisting of two hidden layers and the number of neurons varying in both layers are presented in Figure 5. Here the zero value means that the MSE value of 10^{-4} was reached. If the performance parameter of the MSE validation was not reached, it meant that the training of the FFBN was not successful.

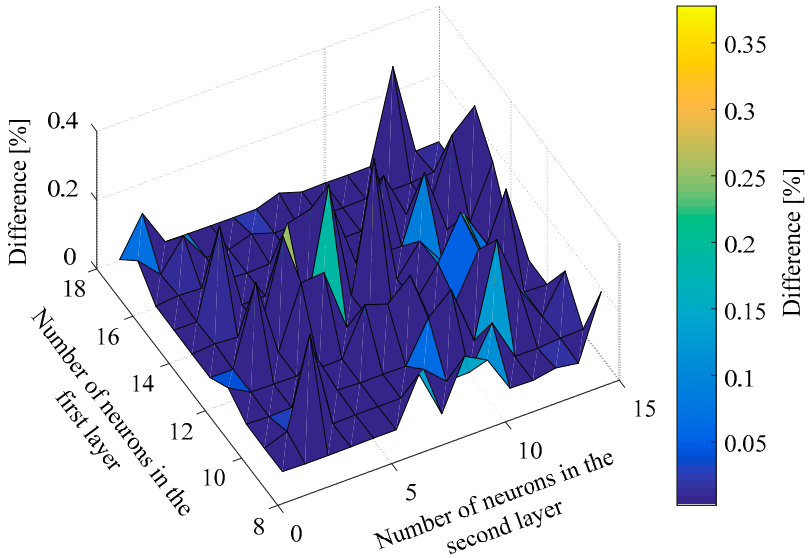

Figure 5. Validation of the feed-forward backpropagation network (FFBN) when the network consisted of two hidden layers.

The best validation results were obtained when the first hidden layer had 18 neurons and the number of neurons varied in the second hidden layer. We then tried to increase the number of hidden layers in the FFBN to three. Based on the validation results presented in Figure 5, we decided to have a constant number of 18 neurons in the first hidden layer and to try to vary the number of neurons in the second and third layers (Figure 6).

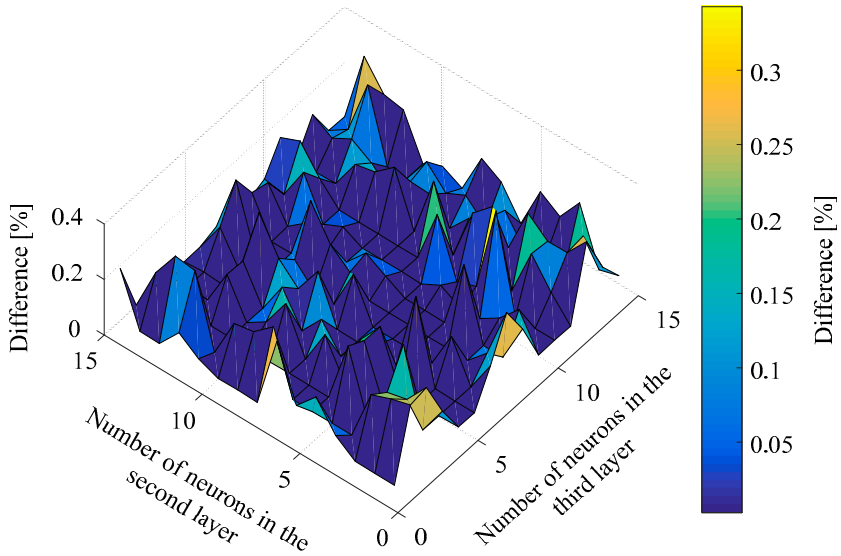

Figure 6. Validation of the FFBN when the network consisted of three hidden layers, when the first layer consisted of 18 neurons.

The best validation results were obtained when the network had 14 neurons in the second hidden layer and 2 neurons in the third hidden layer. The first hidden layer was constant and had 18 neurons.

2.5. Analysis of the Primary Results

The hybrid meander system was designed using Sonnet® software. Previous studies showed that input impedance, retardation factor, and characteristics of the transfer coefficient correlate with

certain results, which were obtained in [30] using the analytical multiconductor line method and the numerical finite-difference time-domain (FDTD) method in CST Microwave Studio® (Figure 7).

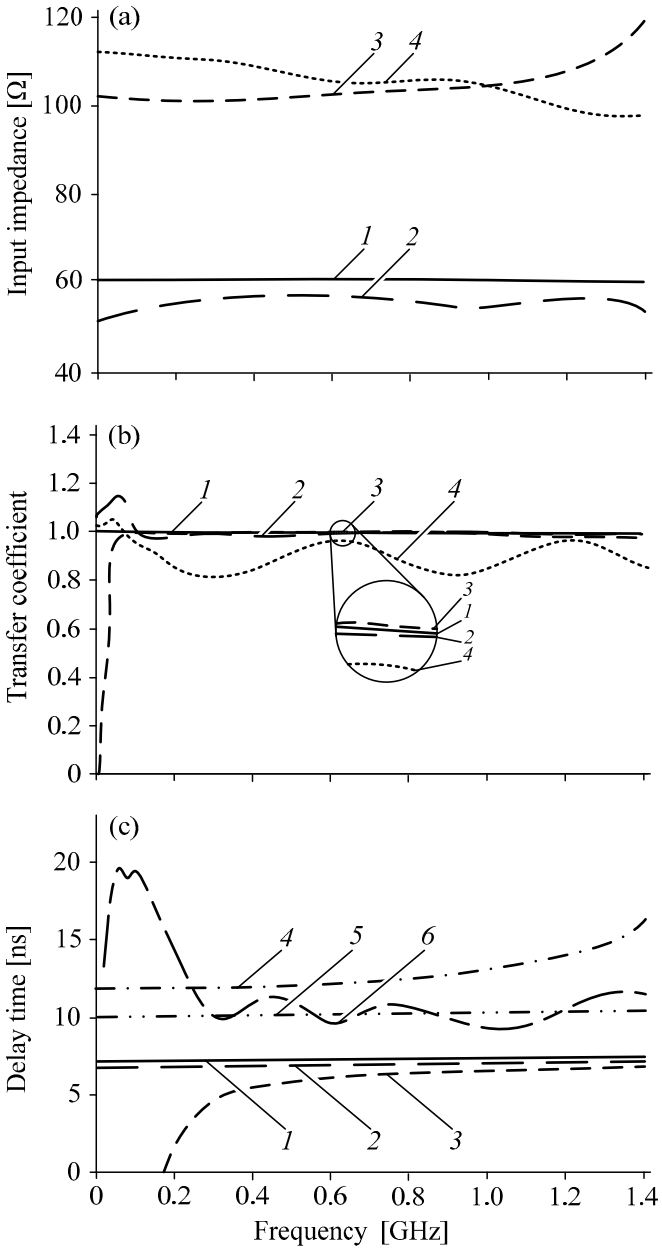

Figure 7. (**a**) The results of the input impedance characteristics: 1 = our developed algorithm, inductance was 0 nH [30]; 2 = Sonnet®; 3 = our developed algorithm, inductance was 5 nH [30]; 4 = Sonnet®. (**b**) The characteristics of the transfer coefficient: 1 = CST Microwave Studio®, inductance was 0 nH; 2 = Sonnet®; 3 = CST Microwave Studio®, inductance was 5 nH; 4 = Sonnet. (**c**) The characteristics of the delay time: 1 = our developed algorithm, inductance was 0 nH [30]; 2 = CST Microwave Studio®; 3 = Sonnet®; 4 = our developed algorithm, inductance was 5 nH [30]; 5 = CST Microwave Studio®; 6 = Sonnet®.

Note that only a few cases are included in Figure 7 for better understandability. Figure 7a represents the results of input impedance when the inductance was 0 or 5 nH. The average value of input impedance was the same with both the analytical multiconductor line method and the MoM, but there was some periodical variation in the results that were obtained using MoM in Sonnet®. Figure 7b represents the results of the transfer coefficient, which were obtained using the FDTD and

MoM methods. The stop band was determined precisely by both methods, when the inductance was 0 nH or 5 nH. The delay time was almost the same using both methods (Figure 7c). The uncertain delay time results started at almost the same stop-band frequency, and the difference was only 40 MHz.

In summary, the results show that it is possible to replace spiral coils with inductive components in the peripheral parts of a meander conductor without losing the properties of the hybrid meander system. The positive results allowed us to design, manufacture, and experimentally investigate the real models of the hybrid meander system.

3. Results

3.1. Experimental Investigation

The inductive components that were used in the modeling process in Sonnet® and the CST Microwave Studio® were replaced with contact plates in the PCB. The 10 nH inductors were soldered to the contact plates in order to simulate spiral coils (Figure 8a).

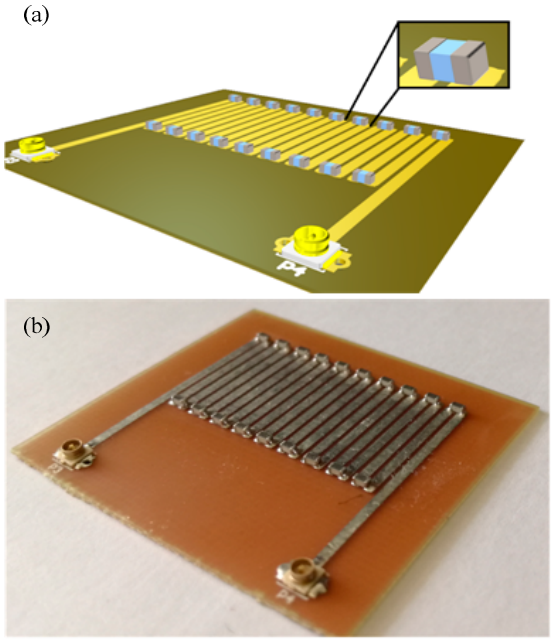

Figure 8. The hybrid meander system: (**a**) PCB model and (**b**) manufactured prototype (zoomed image).

The manufactured hybrid meander system is presented in Figure 8b. FR-4 material was used in the PCB. Here, the FR-4 is a NEMA-grade designation for glass-reinforced epoxy laminate material. The relative permittivity of FR-4 is equal to 4.6. In order to adapt to the manufacturers, a few parameters were adjusted as follows: the step of conductors (L = 1.5 mm), the gaps among the conductors (l = 0.4 mm), the thickness of conductors (t = 0.35 µm), and the gap between the meander electrode and the shield ($w2$ = 0.6 mm). Therefore, a qualitative but non-quantitative comparison can be made between results of the computational modeling and the experimental measurements.

The results of our measurements show that the measured dependencies of the transfer coefficient on frequency were distorted. This can be explained by the fact that the output signal reflected off the mismatched end of the manufactured hybrid meander system, and also that insertion losses were high. The experimental results correlated with the results obtained during the computer-based simulation (Figure 9a). The higher difference between results was achieved when the inductivity of the coils was 10 nH. The characteristics of the transfer coefficient were almost the same as achieved using CST Microwave Studio® and Sonnet® software when the inductivity of the coils was 10 nH (Figure 9b).

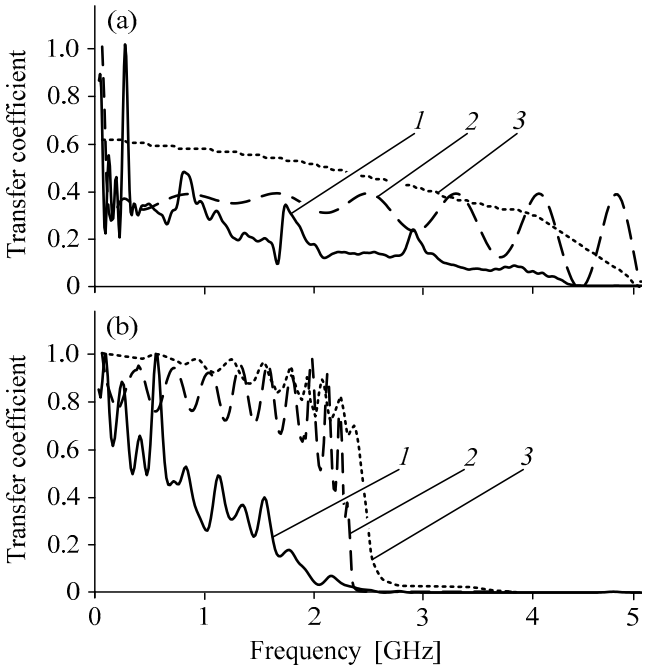

Figure 9. Modeling results and measurements of the hybrid meander systems at (**a**) 0 nH and (**b**) 10 nH, where 1 = measurements, 2 = CST Microwave Studio®, and 3 = Sonnet®.

According to the results shown in Figure 9, it is possible to increase pass-band and input impedance of the slow-wave system using the inductors in the peripheral parts of the meander electrodes. Variations of retardation factor and input impedance of the HMH system were relatively small in the wide frequency range.

3.2. Prediction Results Using the FFBN

We compared the prediction results of the $S_{11}(f)$ and $S_{21}(f)$ parameters obtained using the FFBN with the results of the MoM method (obtained using Sonnet® software). The prediction of S-parameters of the HMH system was performed in three different cases:

- Inductivity of the helical turns $L_i = 10$ nH,
- Inductivity of the helical turns $L_i = 18$ nH,
- Inductivity of the helical turns $L_i = 27$ nH.

The comparison of the S- parameters of the HMH system, which were predicted using FFBN and calculated using the Sonnet® software, are presented in Figure 10. The lowest mean differences between the calculated and predicted $S_{11}(f)$ and $S_{21}(f)$ characteristics were not large—the lowest mean differences were only 6.74% for $S_{11}(f)$, and 4.79% for $S_{21}(f)$. The lowest mean differences between the calculated and predicted results were 6.77% for $S_{11}(f)$ and 4.98% for $S_{21}(f)$ when the structure of the network was 18 × 15 × 4 (18 neurons in the first hidden layer, 15 neurons in the second hidden layer, and 4 neurons in the third hidden layer of the network), and the highest mean differences were 79.79% for $S_{11}(f)$ and 78.53% for $S_{21}(f)$ when the structure of the network was 18 × 8 × 6 and 10 nH inductors were used (Figure 10a). The lowest mean differences between the calculated and predicted results increased—but did not exceed 6.92% for $S_{11}(f)$ or 4.76% for $S_{21}(f)$, $S_{21}(f)$—when the structure of the network was 18 × 10 × 3, and the highest mean differences were 81.90% for $S_{11}(f)$ and 83.7% for $S_{21}(f)$ when the structure of the network was 18 × 7 × 9 and the inductivity of the helical turns was 18 nH (Figure 10b). Finally, the lowest mean differences between the calculated and predicted results decreased down to 6.53% for $S_{11}(f)$ and 4.64% for $S_{21}(f)$ when the structure of the network was 18 × 14 × 2, and the highest mean differences were 84.48% for $S_{11}(f)$ and 76.5% for $S_{21}(f)$ when

the structure of the network was 18 × 15 × 8 and the inductivity of the helical turns was 27 nH (Figure 10c).

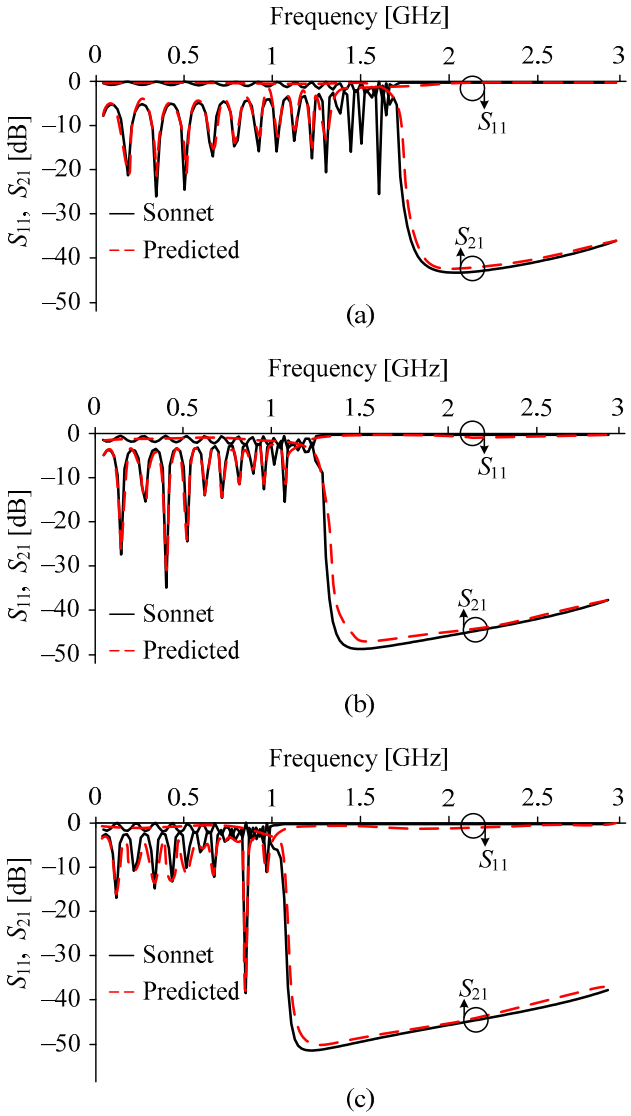

Figure 10. Comparison of the calculated and predicted results of the hybrid meander system when inductivity of the helical turns was (**a**) 10 nH, (**b**) 18 nH, and (**c**) 27 nH.

The comparison of the predicted and calculated results also showed that the cut-off frequencies of the $S_{11}(f)$ and $S_{21}(f)$ parameters were the same in both cases at the −3 dB level.

The influence of the number of neurons in the hidden layers of the FFBN on the predicted results of the S-parameters is presented in Figure 11. The highest difference between the calculated (using Sonnet® software) and the predicted S-parameters were obtained when the inductivity of the helical turns was 18 nH (the difference between results was 82.8%). The highest difference between results was obtained when the structure of the FFBN was 18 × 7 × 9 (18 neurons in the first hidden layer, 7 neurons in the second hidden layer, and 9 neurons in the third hidden layer of the network) (see Figure 11b).

The lowest difference between results was achieved when the structure of the FFBN was 18 × 14 × 2 (18 neurons in the first hidden layer, 14 neurons in the second hidden layer, and 2 neurons in the third hidden layer of the network) (Figure 11c), while the inductivity of the helical turns was equal to 27 nH. The influence of these differences on the performance of the HMH system was small.

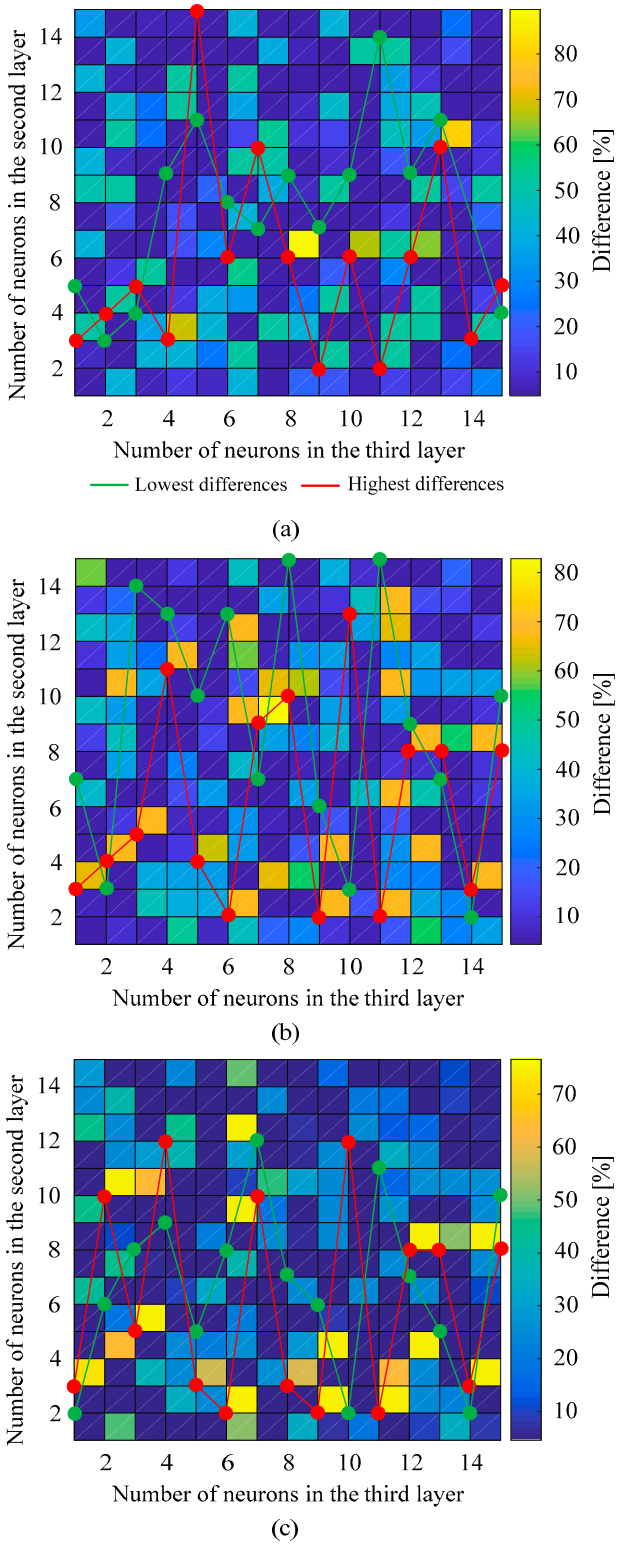

Figure 11. Relationship between the number of neurons in the hidden layers of the FFBN and the prediction results when inductivity of the helical turns was (**a**) 10 nH, (**b**) 18 nH, and (**c**) 27 nH.

The calculations were performed much faster than could be accomplished using the Sonnet® software. The prediction of the S-parameters of the hybrid meander system using the FFBN was performed on a computer with the following parameters: Intel Core i7-2820QM @ 2.30GHz with 16 GB of RAM and an NVIDIA GeForce GT 630 2 GB RAM video card. The calculation time was equal to 8 h

using the MoM method (using Sonnet® software). The prediction time was 127.43 s using the FFBN, which was much faster than using the MoM method. The training process of the FFBN took less than 63 s.

4. Conclusions

We used the feed-forward backpropagation network (FFBN) to predict the parameters of hybrid meander systems. The mean differences between the predicted and calculated results differed by less than 6.74% for the $S_{11}(f)$ parameter, and less than 4.79% for the $S_{21}(f)$ parameter. The prediction of parameters using the FFBN was noticeably faster than the calculations using the method of moments (MoM).

The results of modeling and the physical experiment of the hybrid meander system demonstrated that it is possible to increase the pass-band and input impedance of a slow-wave system using the hybrid meander system with the inductors in the peripheral parts of meander electrodes. The spiral coils of the hybrid meander system could be replaced with inductive components in the peripheral parts of the meander conductor without worsening the characteristics of the hybrid meander system.

Author Contributions: Conceptualization, D.P. and A.K. (Andrius Katkevičius); Funding acquisition, D.P.; Investigation, A.K. (Audrius Krukonis) and V.Š.; Methodology, A.K. (Andrius Katkevičius) and A.K. (Audrius Krukonis); Software, A.K. (Audrius Krukonis); Validation, V.Š.; Writing—original draft, D.P. and A.K. (Andrius Katkevičius); Writing—review & editing, R.M. and R.D.

Funding: This research received no external funding.

Acknowledgments: We are very grateful to JSC "Geozondas" for their help in organizing and conducting experimental measurements.

Conflicts of Interest: The authors declare no conflict of interest.

References

1. Ma, T.G.; Wang, C.W.; Lai, C.H.; Tseng, Y.C. *Synthesized Transmission Lines: Design, Circuit Implementation, and Phased Array Applications*; John Wiley & Sons Ltd.: Hoboken, NJ, USA, 2016; pp. 26–60.
2. Menargues, E.; Chudzik, M.; Arnedo, I. Fast Synthesis of Microwave Devices with Arbitrary Frequency Responses and Smooth Profiles. In Proceedings of the 44th European Microwave Conference, Rome, Italy, 6–9 October 2014; pp. 1083–1086.
3. Zhang, R.; Luo, S.; Zhu, L. Synthesis and Design of Mixed Lumped and Distributed Low-Pass Filters/Low-Passing Impedance Transformers with Taylor Series. *IEEE Trans. Microw. Theory Tech.* **2016**, *64*, 1265–1272. [CrossRef]
4. Guo, T.; Zhang, Q.; Chen, Y.; Wang, R.; Caloz, C. Single-Step Tunable Group Delay Phaser for Spectrum Sniffing. *IEEE Microw. Wirel. Compon. Lett.* **2015**, *25*, 808–810. [CrossRef]
5. Ratnaparkhi, V.V.; Deshmukh, K.N. Design and performance analysis of microwave amplifier using S-Parameters. In Proceedings of the International Conference on Global Trends in Signal Processing, Information Computing and Communication, Jalgaon, India, 22–24 December 2016; pp. 631–633.
6. Katkevičius, A.; Štaras, S. Analysis of rejection properties of meander systems. *Electron. Electr. Eng.* **2011**, *108*, 19–22. [CrossRef]
7. Qian, C.; Ding, D.; Bi, J.; Chen, R. Numerical Analysis of Multi-Carrier Microwave Breakdown in Waveguide Components. *IEEE Microw. Wirel. Compon. Lett.* **2016**, *26*, 77–79. [CrossRef]
8. Tamma, V.A.; Figotin, A.; Capolino, F. Concept for Pulse Compression Device Using Structured Spatial Energy Distribution. *IEEE Trans. Microw. Theory Tech.* **2016**, *64*, 742–755. [CrossRef]
9. Zhou, H.W.; Yang, X.X.; Rahim, S. Synthesis of the Sparse Uniform-Amplitude Concentric Ring Transmitting Array for Optimal Microwave Power Transmission. *Int. J. Antennas Propag.* **2018**, *2018*, 8075318. [CrossRef]
10. Wang, Y.; Zhu, L.; Wang, H.; Yang, G. Design of Compact Wideband Meandering Loop Antenna with a Monopole Feed for Wireless Applications. *Prog. Electromagn. Res. Lett.* **2018**, *73*, 1–8. [CrossRef]
11. Alon, L.; Lattanzi, R.; Lakshmanan, K.; Brown, R.; Deniz, C.M.; Sodickson, D.K.; Collins, C.M. Transverse slot antennas for high field MRI. *Magn. Reson. Med.* **2018**, *80*, 1233–1242. [CrossRef]

12. Sánchez-Montero, R.; Camacho-Gómez, C.; López-Espí, P.L.; Salcedo-Sanz, S. Optimal Design of a Planar Textile Antenna for Industrial Scientific Medical (ISM) 2.4 GHz Wireless Body Area Networks (WBAN) with the CRO-SL Algorithm. *Sensors* **2018**, *18*, 1982. [CrossRef]
13. Guan, C.; Kanaya, H. 360° Phase Shifter Design Using Dual-Branch Switching Network. *IEEE Microw. Wirel. Compon. Lett.* **2018**, *28*, 675–677. [CrossRef]
14. Tobia, A.; Ramaccia, D.; Toscano, A.; Bilotti, F. Design and Experimental Verification of a Compact Gaussian Beam Source for Parallel-Plate Waveguide Tests. *IEEE Trans. Antennas Propag.* **2018**, *66*, 4288–4291. [CrossRef]
15. Gulyaev, Y.V.; Mityagin, A.Y.; Chuchevab, G.V.; Afanas'ev, M.S. Principles of Creation of Microwave Delay Lines Based on Nanoscale Ferroelectric Films. *J. Commun. Technol. Electron.* **2014**, *59*, 87–92. [CrossRef]
16. Pomarnacki, R.; Krukonis, A.; Urbanavičius, V. Acceleration Techniques for Analysis of Microstrip Structures. *Electron. Electr. Eng.* **2014**, *20*, 108–111. [CrossRef]
17. Villeneuve, R.; Cueille, M.; Arnaud-Cormos, D.; David, J.-F.; Leveque, P.; Durand, A.-J. Setup and Characterization of a Backward Wave Oscillator Delay Line Scaled Down to Centimeter and Millimeter-Wave Ranges. *IEEE Trans. Terahertz Sci. Technol.* **2015**, *5*, 1053–1061. [CrossRef]
18. Gavrilovic, M.M.; Webb, J.P. Accuracy control in the optimization of microwave devices by finite-element methods. *IEEE Trans. Microw. Theory Tech.* **2002**, *50*, 1901–1911. [CrossRef]
19. Ghayoula, E.; Ghayoula, R.; Haj-Taieb, M.; Chouinard, J.Y.; Bouallegue, A. Pattern Synthesis Using Hybrid Fourier-Neural Networks for IEEE 802.11 MIMO Application. *Prog. Electromagn. Res. B* **2016**, *67*, 45–58. [CrossRef]
20. Hassan, N.; Yassin, A.; Tayer, M.; Mohamed, M.M. Ultra-wideband Scattered Microwave Signals for Detection of Breast Tumors Using Artificial Neural Networks. In Proceedings of the International Conference on Artificial Intelligence and Pattern Recognition (AIPR2016), Lodz, Poland, 19–21 September 2016; pp. 137–142.
21. Huang, A.-D.; Zhong, Z.; Wu, W.; Guo, Y.-Z. An Artificial Neural Network-Based Electrothermal Model for GaN HEMTs With Dynamic Trapping Effects Consideration. *IEEE Trans. Microw. Theory Tech.* **2016**, *64*, 2519–2527. [CrossRef]
22. Keerthan, P.; Kumar, R.; Vinoy, K.J. A Novel All-Pass Network Implementation for Improved Group Delay Performance. *IEEE Microw. Wirel. Compon. Lett.* **2016**, *26*, 804–806. [CrossRef]
23. Liu, W.; Na, W.; Zhu, L.; Ma, J.; Zhang, Q.J. Wiener-Type Dynamic Neural Network Approach to the Modeling of Nonlinear Microwave Devices. *IEEE Trans. Microw. Theory Tech.* **2017**, *65*, 2043–2062. [CrossRef]
24. Liu, W.; Na, W.; Zhu, L.; Zhang, Q.J. A Review of Neural Network Based Techniques for Nonlinear Microwave Device. In Proceedings of the IEEE MTT-S International Conference on Numerical Electromagnetic and Multiphysics Modeling and Optimization, Beijng, China, 27–29 July 2016; pp. 1–2.
25. Singhal, M.; Saini, G. Optimization of Antenna Parameters Using Artificial Neural Network: A Review. *Int. J. Comput. Trends Technol.* **2017**, *44*, 64–73. [CrossRef]
26. Połap, D.; Woźniak, M.; Wei, W.; Damaševičius, R. Multi-threaded learning control mechanism for neural networks. *Future Gener. Comput. Syst.* **2018**, *87*, 16–34. [CrossRef]
27. Ghorbaninejad, H.; Heydarian, R. New Design of Waveguide Directional Coupler Using Genetic Algorithm. *IEEE Microw. Wirel. Compon. Lett.* **2016**, *26*, 86–88. [CrossRef]
28. Erredir, C.; Riabi, M.L.; Ammari, H.; Bouarroudj, E. Design of Waveguide Structures Using Improved Neural Networks. *J. Microw. Optoelectron. Electromagn. Appl.* **2017**, *16*, 900–907. [CrossRef]
29. Panagiotou, S.C.; Thomopoulos, S.C.A.; Capsalis, C.N. Genetic Algorithms in Antennas and Smart Antennas Design Overview: Two Novel Antenna Systems for Triband GNSS Applications and a Circular Switched Parasitic Array for WiMax Applications Developments with the Use of Genetic Algorithms. *Int. J. Antennas Propag.* **2014**, *2014*, 729208. [CrossRef]
30. Daškevičius, V.; Skudutis, J.; Katkevičius, A.; Štaras, S. Simulation and properties of the wide-band hybrid slow-wave system. *Electron. Electr. Engineer.* **2010**, *104*, 43–46.